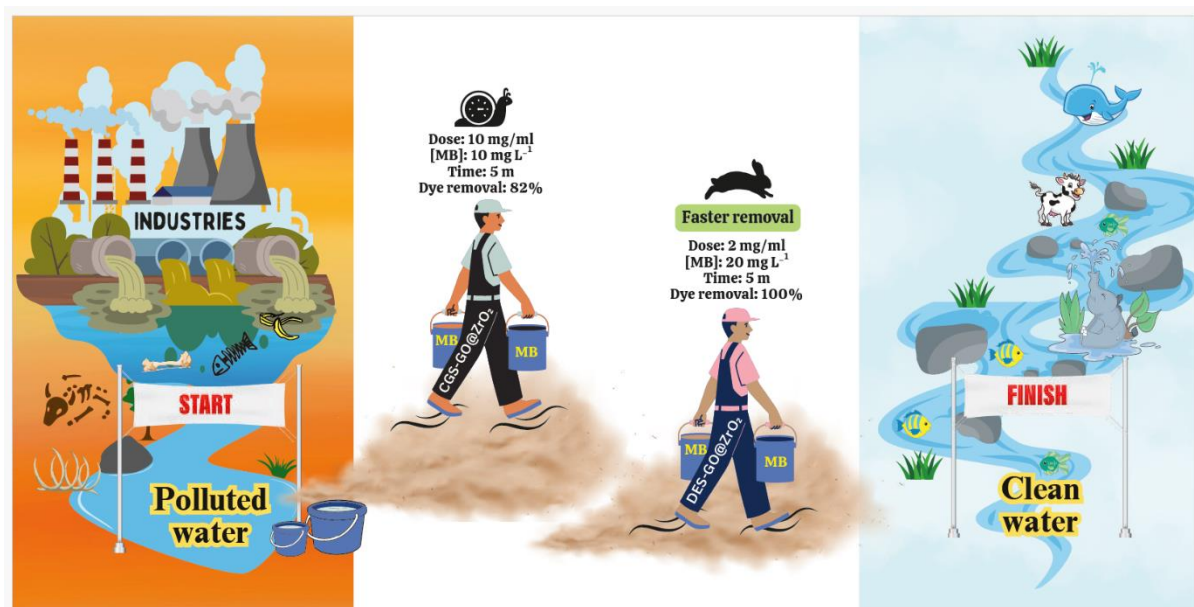


Synthesis and characterization of surfactant/DES modified GO@ZrO₂ NC for adsorption of dye from aqueous background

Contents

- 3.1 Introduction
- 3.2 Experimental section
- 3.3 Results and Discussion
 - 3.3.1 XRD Patterns
 - 3.3.2 FTIR spectroscopy
 - 3.3.3 TEM analysis
 - 3.3.4 SEM-EDX analysis
 - 3.3.5 Thermogravimetric analysis
 - 3.3.6 Influence of [MB]
 - 3.3.7 Influence of Composite Load
 - 3.3.8 Influence of pH
 - 3.3.9 Influence of Contact Time: Adsorption Kinetics
 - 3.3.10 Adsorption isotherm
 - 3.3.11 Comparison of MB adsorption with similar composite material
 - 3.3.12 Recyclability/Reusability Study
 - 3.3.13 Mechanism of MB adsorption
- 3.4 Conclusion

This chapter is mainly focused on covalent functionalization of GO@ZrO₂ through surfactants and DES. The modified NCs is characterized using FTIR, XRD, TEM, SEM-EDX and TGA. The dye adsorption study of the prepared NCs is also discussed in this chapter. The modified NCs is a suitable material for waste water treatment.



3.1 Introduction

As previously discussed, carbon allotropes have gained significant attention over the last few decades for their unique properties and diverse applications [1–11]. Graphene, a uni-layer bi-dimensional surface of carbon atoms in sp² configuration, is widely used in pure form or as composites in various scientific and engineering applications [4,12–15]. Despite graphene's exceptional mechanical, electrical, and thermal properties [16], graphene oxide (GO) is preferred due to its functional groups. GO exhibits spontaneous distribution in aqueous media, making it useful for polluted water treatment [17,18]. However, challenges arise from its high surface energy leading to agglomeration and lower dispersibility [19]. To address these issues, GO is often fused with metallic oxides, forming nanocomposite (NC) that modify its properties [20–24]. NCs, characterized by multicomponent materials with different phase nano-domains, exhibit specific architectural morphology and photochemical characteristics beneficial for water treatment technologies [25].

ZrO₂, among various metal oxides used for composite formation, attracts researchers due to its passive nature, lower reductive potential, and lower processing cost [26]. GO-based metal composites are effective for removing cationic pollutants but less so for anionic moieties [27]. To enhance the efficiency of NCs, they are modified with a variety of compounds, including synthetic and natural polymers, and surfactants [27–34].

As discussed in previous chapters, surfactants serve as preferred modification agents, simplifying the synthesis process and improving crystallinity/thermal stability, preventing agglomeration, and increasing surface area and controlled porosity [35–40]. Cationic surfactants, especially cationic gemini surfactant (CGS), have shown promise as modifiers, displaying improved structural and surface/solution properties over conventional cationic surfactants [41–46]. CGS-modified NCs, involving metal oxides and GO, have demonstrated effectiveness in adsorption/degradation phenomena [33,47]. Deep eutectic solvents (DESs) are gaining momentum as modifiers in nanomaterial synthesis, processing, and functionalization of NCs [48–51]. DES, known for being safe, accessible, green, and environmentally friendly, exhibits increased affinity towards materials of interest [52,53].

In this chapter, our primary focus has been on tackling the formidable challenge of preserving pure water bodies for the next generation on Earth an issue recognized as the most significant facing the research community [54–58]. World Bank data underscores the critical role of textile waste, contributing approximately 20% to total industrial water pollution, particularly through color or color-causing materials [59]. Consequently, the elimination of color and coloring compounds from industrial effluents stands out as the foremost requirement encountered by industries worldwide. This imperative has driven the search for an optimized treatment method to mitigate coloring pollutants from effluents before their integration into regular potable water streams. NCs have emerged as a potential solution to this challenge, leveraging various modifications [20,60–64]. Capitalizing on the economic and synthetic characteristics of ZrO₂ and DES, both were strategically chosen for NC synthesis with GO and subsequent functionalization, leading to the creation of DES-GO@ZrO₂. Furthermore, another analogous composite was synthesized and modified with CGS using a method reported elsewhere [33]. In this study, butanediyl-1,4, bis (N, N-hexadecyl ammonium) dibromide (16-4-16) and reline were employed as CGS and DES, respectively [65]. The modified NCs underwent comprehensive characterization through various instrumental methods. To optimize their performance, various experimental conditions were systematically adjusted. Notably, this chapter presents, a comparative study on CGS/DES modified NCs, offering valuable insights into their effectiveness. The strategies and methodologies detailed in this chapter hold promising applications in addressing water pollution

and contributing to environmental cleanup efforts. By effectively reducing dye content in aqueous media, these approaches offer a meaningful contribution towards ensuring a cleaner and more sustainable environment.

3.2 Experimental section

The materials and methods used are discussed in chapter 2.

3.3 Result and discussion

3.3.1 XRD

Crystallinity of the NCs were analyzed using XRD. The XRD spectra of all the NCs are shown in **Figure 3.1**. The broadness of NC spectra indicates poor crystallinity (amorphousness) of all NCs. When XRD data were compared with pure GO and pure ZrO₂, the composite material has been found more amorphous than individual components. Similar types of signals were observed for the controlled deposition of ZrO₂ on graphene nanosheets in earlier studies [66,67]. Data shows that amorphousness more or less remained similar even after modification with CGS or DES. In an earlier study, it has been shown that surfactant modified NC-material shows amorphousness more than pure GO and corroborates the present data [68].

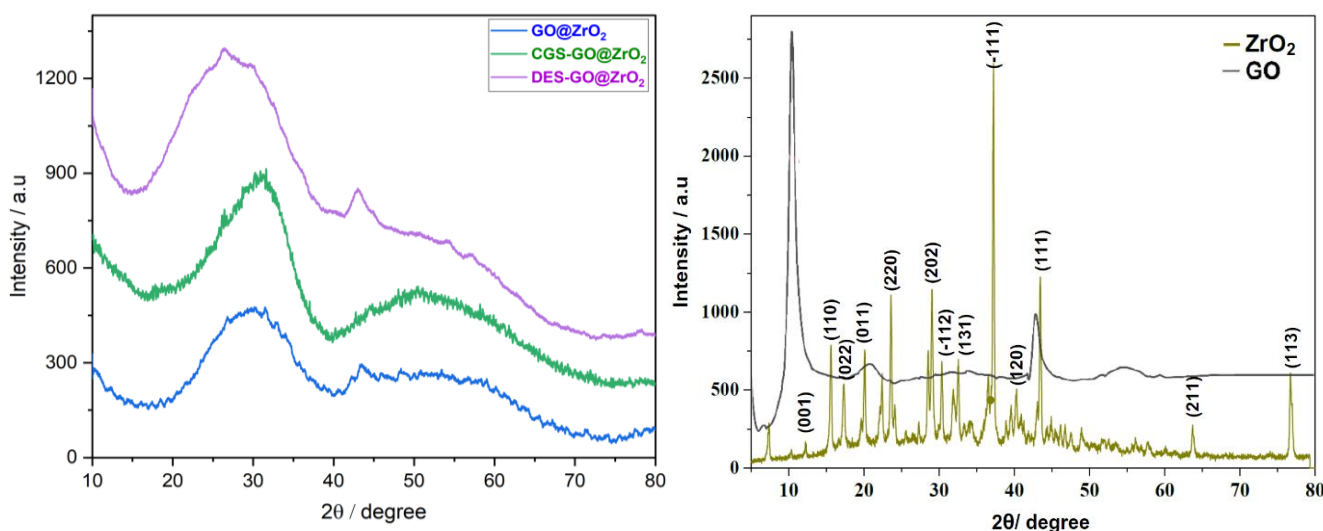


Figure 3.1: XRD spectra of modified nanocomposite(s) and its precursor.

3.3.2 FTIR

FTIR spectra for GO@ZrO₂, CGS-GO@ZrO₂, and DES-GO@ZrO₂ are compiled in **Figure 3.2**. The appearance of peaks with CGS-GO@ZrO₂ around 2923 and 2847 cm⁻¹ indicates the existence of C-H stretching vibration bands and confirms the presence of CGS alkyl group

and hence the modification of GO@ZrO₂ by CGS. Similarly, in the case of DES-GO@ZrO₂, peaks are appearing at 3019 and 3261 cm⁻¹ which are expected from the vibrations of H-bonds in O-H and/or N-H, as reported earlier [69]. Further, Zr-O bands are appeared at 635 cm⁻¹ and 762 cm⁻¹. The absorption band appeared at 2900 cm⁻¹ indicating a small alkyl chain of choline part of reline present at the surface of DES-GO@ZrO₂.

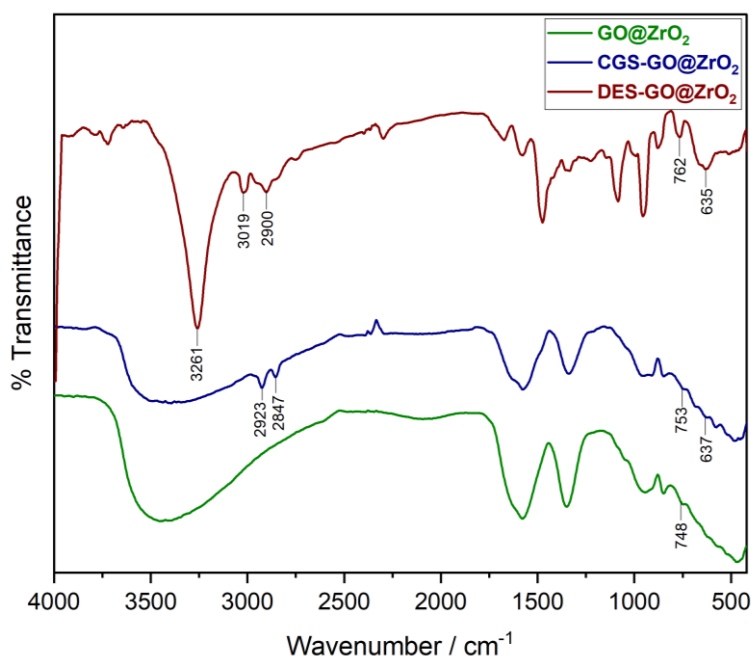


Figure 3.2: FT-IR spectra of GO@ZrO₂ and its modified forms with CGS and DES nanocomposites.

3.3.3 TEM

TEM images of pure GO@ZrO₂ and modified NCs are shown in **Figure 3.3 (a-c)**. Modified composite images (**Figure 3.3 (b & c)**) show wrinkles and folding on the outer part of the original composite. The sheets are comparatively well separated for DES-GO@ZrO₂ than CGS-GO@ZrO₂ (for the same magnification).

3.3.4 SEM-EDX

SEM-EDX data are given in **Figure 3.4 (a-c)** to further ensure the modification of GO@ZrO₂. The elemental analysis data are summarized in the supplementary information (**Table 3.1**). The presence of nitrogen and chlorine atoms in the modified composites shows the functionalization of GO@ZrO₂ with CGS or DES (as the case may be). The data are indicative of the successful functionalization of the GO@ZrO₂ NC.

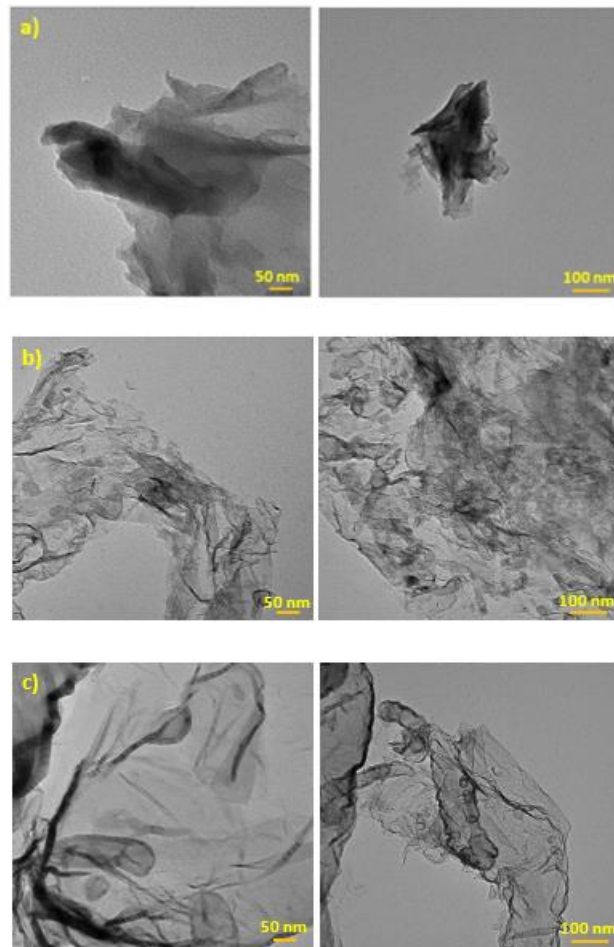


Figure 3.3: TEM images of a) GO@ZrO₂ b) CGS-GO@ZrO₂, and c) DES-GO@ZrO₂.

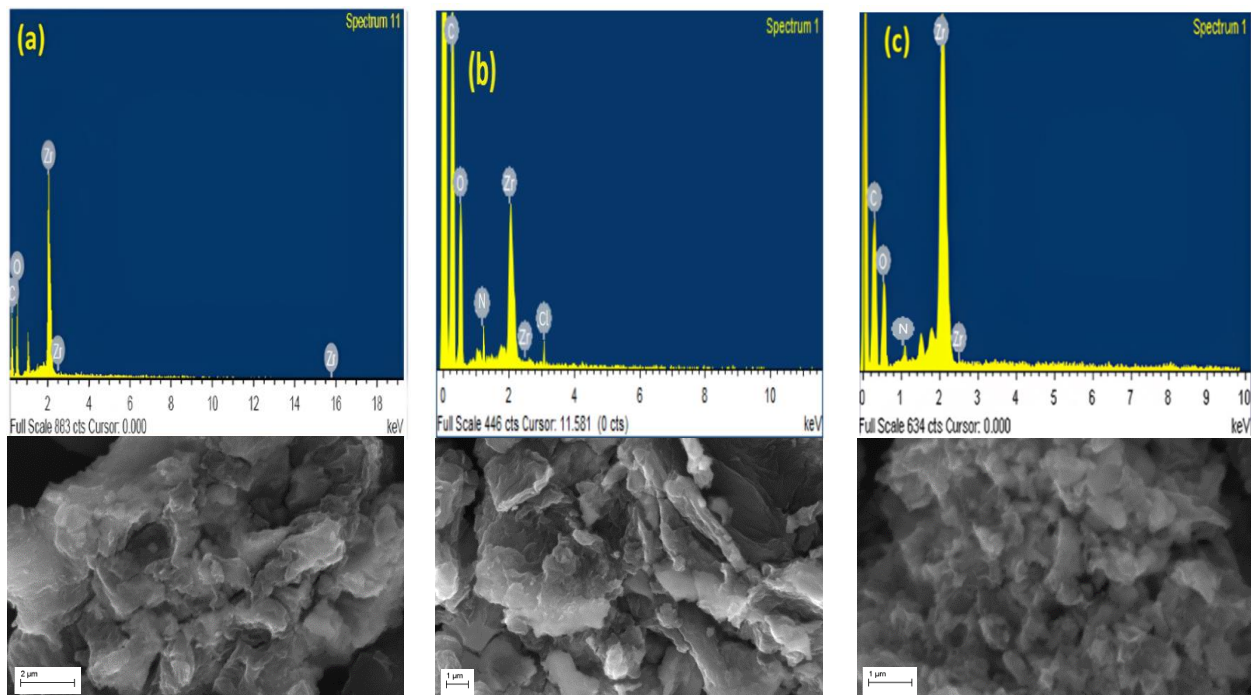


Figure 3.4: SEM-EDX images of a) GO@ZrO₂, b) DES-GO@ZrO₂ and c) CGS-GO@ZrO₂.

Table 3.1: EDX elemental data of modified GO@ZrO₂ with CGS and DES.

Elements	GO@ZrO ₂		CGS-GO@ZrO ₂		DES-GO@ZrO ₂	
	Weight %	Atomic %	Weight %	Atomic %	Weight %	Atomic %
C	42.43	60.75	50.76	69.58	52.48	68.22
O	30.22	33.94	25.58	25.75	23.52	26.30
Zr	27.35	5.31	23.66	4.67	22.75	4.48
N	-	-	-	-	0.96	0.58
Cl	-	-	-	-	0.29	0.42

3.3.5 TGA

TGA thermograms and derivative thermograms for pure and functionalized NCs are provided in Figure 3.5 (a) and (b), respectively. Thermal stability of GO@ZrO₂ increases with both CGS/DES modified NCs. This additional thermal stability in the presence of both DES and CGS indicates that the decomposition of labile surface oxygens is restricted. This surface stability can be further utilized for higher temperature adsorption if needed.

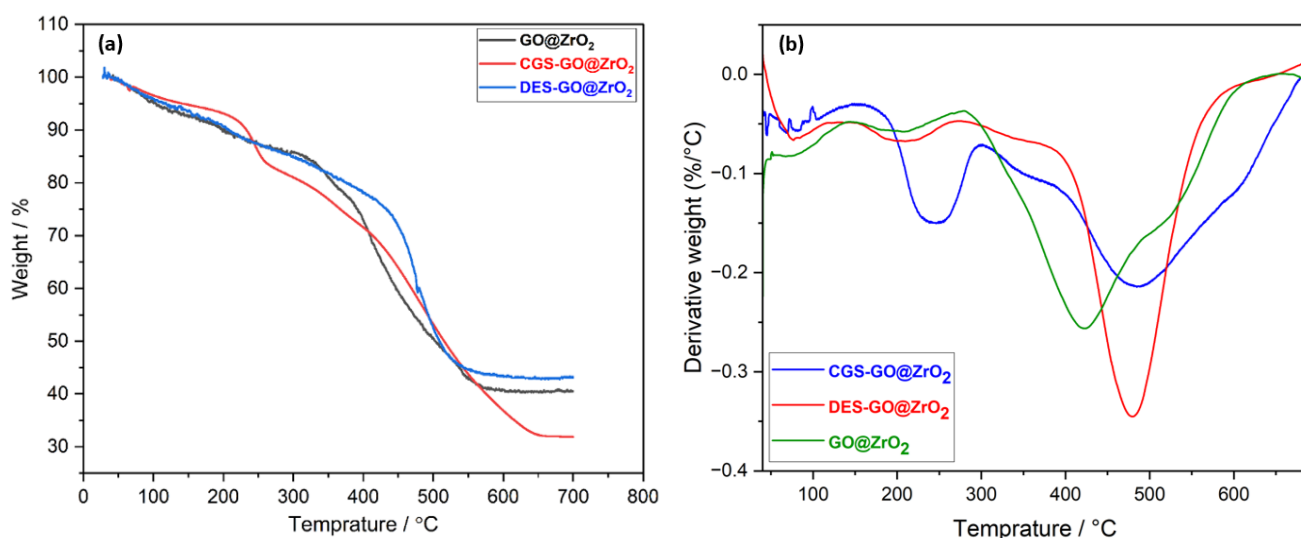


Figure 3.5: a) Thermograms and b) derivative thermograms of GO@ZrO₂ and CGS/DES modified nanocomposites.

3.3.6 Influence of [MB]

Removal of MB (by adsorption process) from aqueous dye solution (without agitation) was studied in the presence of a fixed dose of composite (GO@ZrO₂ (2 mg/ml), CGS-GO@ZrO₂ (10 mg/ml) or DES-GO@ZrO₂ (2 mg/ml)). The percentage of MB removal (P) in all the cases (after 60 m, followed by centrifugation) has been plotted against different fixed [MB] (20-100 mg

L⁻¹), and data are depicted in **Figure 3.6**. The perusal of data suggests that modification improves P value than observed with GO@ZrO₂. It may be mentioned that DES-GO@ZrO₂, even having 5 times lower quantity, competes well for initial lower [MB] (~40 mg L⁻¹). However, at further higher [MB], the P values show distinct differences for the above two modified NCs. Preliminary adsorption data show the competitiveness of DES modified NC with CGS one. In this experiment, the best performances of MB adsorption were found at 20 mg L⁻¹ and 50 mg L⁻¹ for DES-GO@ZrO₂ and CGS-GO@ZrO₂, respectively. Therefore, these concentrations were taken to optimize the composite dosages.

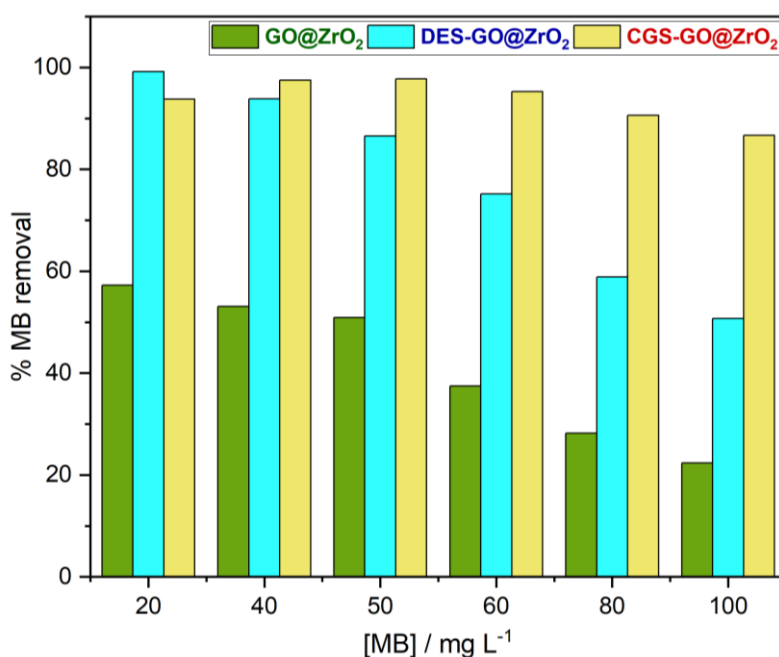


Figure 3.6: Variation of % MB removal from background solution (20 ml, after 60 m) with different initial concentrations of MB (20-100 mg L⁻¹) at 30±0.1°C: GO@ZrO₂ (2 mg/ml); DES-GO@ZrO₂ (2 mg/ml) and CGS-GO@ZrO₂ (10 mg/ml).

3.3.7 Influence of Composite Load

Above fixed MB concentrations were used to study the influence of composite load on the absorbability of MB from an aqueous solution. NC load has been varied to determine the appropriate content of the adsorbent in the removal of MB (after 60 m) together with Q. Data for DES-GO@ZrO₂ and CGS-GO@ZrO₂ are shown in **Figure 3.7**. A perusal of the data indicates that a near complete MB adsorption has been observed at/above 2 mg/ml with the former NC while similar MB adsorption was observed at/above 10 mg/ml for the latter NC (CGS-GO@ZrO₂). Therefore, 2 mg/ml composite load and 20 mg L⁻¹ MB concentration have been fixed for DES-GO@ZrO₂ while 10 mg/ml composite load and 50 mg L⁻¹ MB concentration were fixed with CGS-GO@ZrO₂ for pH effect.

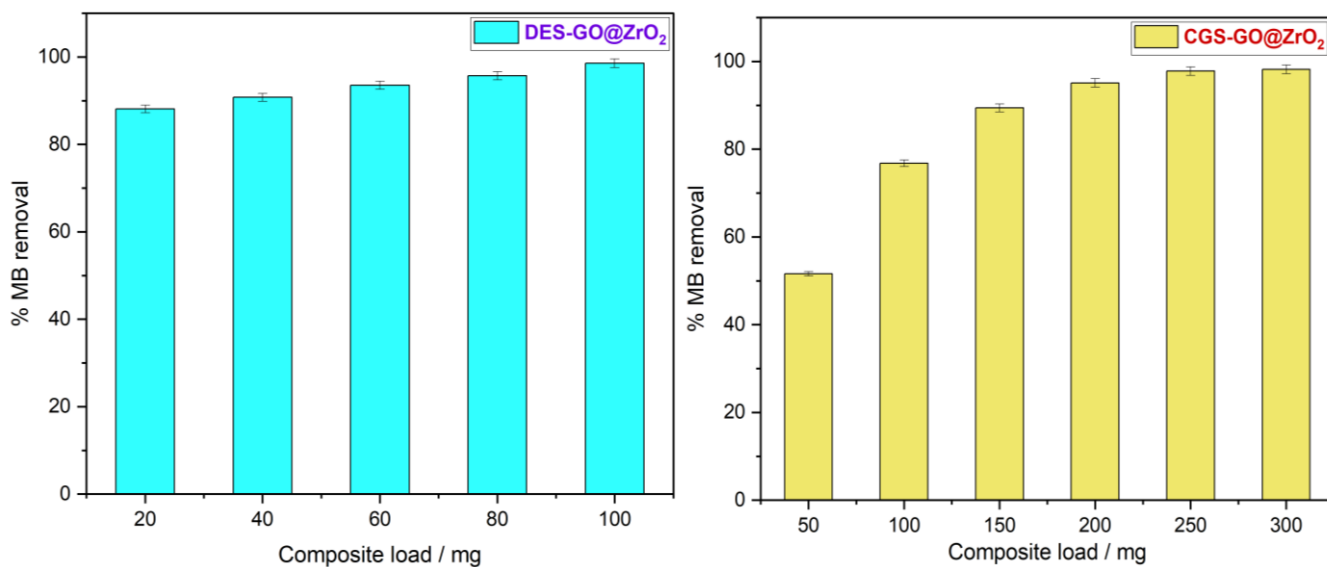


Figure 3.7: Optimisation of composite dosages for MB adsorption (20 ml solution, after 60 m): DES-GO@ZrO₂ (with 20 mg L⁻¹ MB) and CGS-GO@ZrO₂ (with 50 mg L⁻¹ MB) at 30±0.1°C.

3.3.8 Influence of pH

pH variation has been accomplished by varying the concentration of NaOH/HCl depending upon the pH range (basic or acidic). With an increase in pH, MB molecules will exist in both charged and uncharged forms. The variation of P vs pH for the above-mentioned systems (after 60 m) has been shown in **Figure 3.8**. P has been found lower in a higher acidic range which increases with an increase in pH and shows distinctly higher MB adsorption (or P) at pH 10 for DES-GO@ZrO₂. This may be interpreted in terms of the conversion of cationic MB form into neutral MB form. The latter form may be driven towards NC surface due to the hydrophobic attraction of the dye towards modified NC surfaces. **Figure 3.9** shows the variation of ΔpH vs pH_{initial} and resulted in pH_{pzc} zero between pH 7 to 8. After this pH range the NC surface will behave negatively charge and start attracting the cationic form of the dye and responsible for a sudden increase in the P value from pH 8-10. This could also be understood in light of the fact that the pK_a value of MB is 3.8 [70]. The increase in P value with pH finds support from an earlier study in which MB adsorption has been made on a GO-based composite [71]. However, the amount of MB adsorbed from pH 4-8 for CGS-GO@ZrO₂ is nearly constant. The former form will interact electrostatically with the CGS-GO@ZrO₂ surface while the latter one will interact hydrophobically. The overall adsorption might be the result of the above two interactions and works oppositely for CGS-GO@ZrO₂ and is responsible for a level-off in the P value. This is indeed observed in **Figure 3.8**.

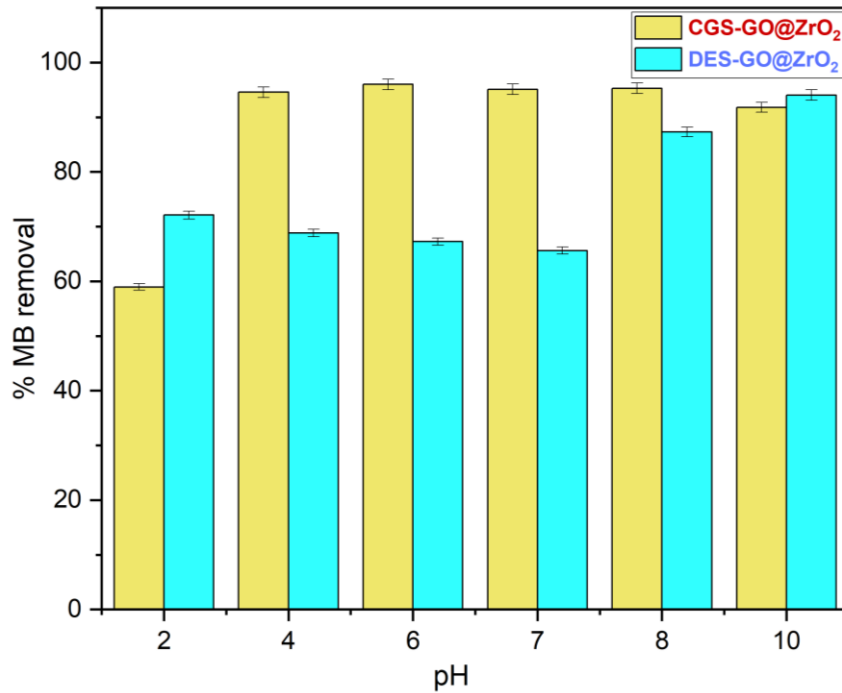


Figure 3.8: Influence of pH (2-10) on MB adsorption (20 ml solution, after 60 m) by DES-GO@ZrO₂ (2 mg/ml dosage, with 20 mg L⁻¹ MB) and b) CGS-GO@ZrO₂ (10 mg/ml dosage, with 50 mg L⁻¹ MB) at 30±0.1°C.

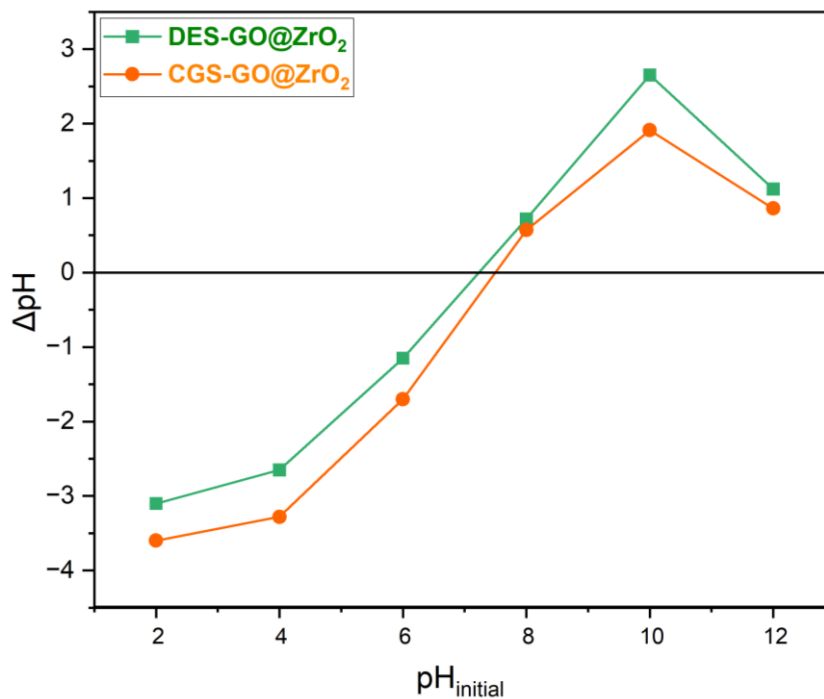


Figure 3.9: Variation of ΔpH vs pH_{initial} for DES-GO@ZrO₂ (50 mg/20 ml KNO₃ solution) and CGS-GO@ZrO₂ (50 mg/20 ml KNO₃ solution) at 30±0.1°C.

3.3.9 Influence of Contact Time: Adsorption Kinetics

In order to understand the kinetics of the adsorption process, influences of contact time and [MB] have been seen at a fixed concentration of composite (2 or 10 mg/ml) and pH (=10). Q_t values at different time intervals (Q_t) are plotted against time (t) and such profiles are shown in **Figure 3.10 (a & b)**. The data have been used to obtain Q_e (amount of MB adsorbed per gram of composite after attaining equilibrium). Various kinetic models (pseudo-first order, pseudo-second order, and intraparticle diffusion model) have been applied to reveal adsorption kinetics. Following the well-known Lagergren equation is widely used for liquids and solid systems to deal with pseudo-first order kinetics [72].

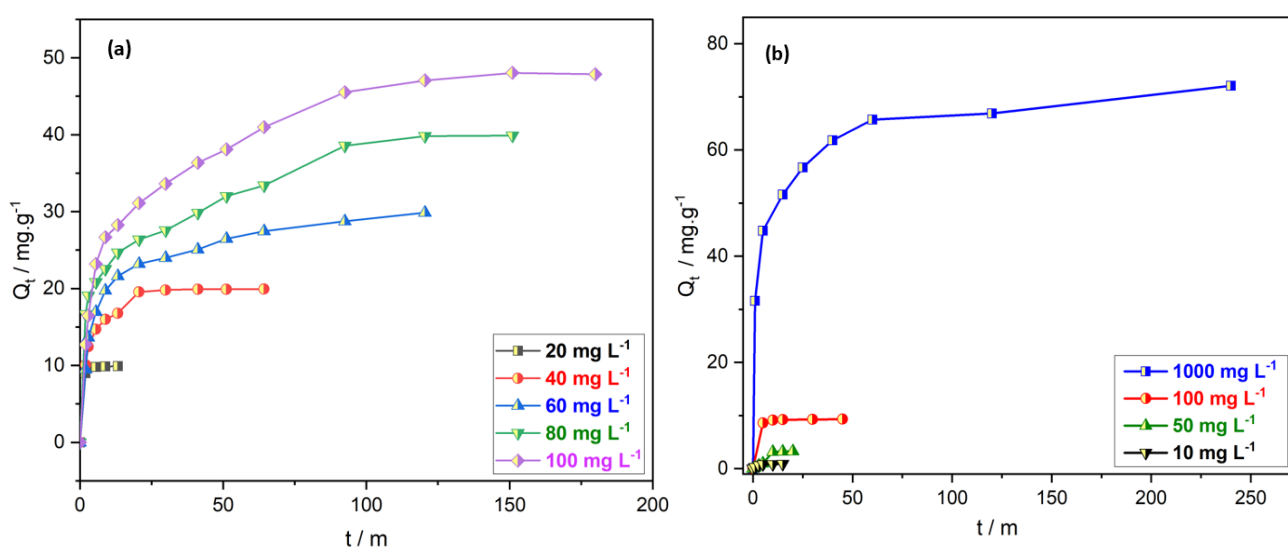


Figure 3.10: Variation of adsorption capacity (Q_t) with Contact time (t) for various starting MB concentrations (10-1000 mg L⁻¹): a) DES-GO@ZrO₂ (2 mg/ml dosage, 20 ml solution of MB), and b) CGS-GO@ZrO₂ (10 mg/ml dosage, 20 ml solution of MB) at 30±0.1°C.

3.3.9.1 Pseudo-first order kinetic model

$$\ln(Q_e - Q_t) = \ln Q_e - k_1 t \quad (1)$$

where k_1 (min⁻¹) represents the pseudo-first order rate constant for the MB adsorption. Q_e and k_1 can be obtained from the slope and intercept of $\log(Q_e - Q_t)$ vs t plots (**Figure 3.11 (a & b)**). The computed data related to this model are compiled in **Table 3.2**. A perusal of **Figure 3.10** clearly depicts that kinetic data cannot be fitted in the present model (with both the NCs, **Table 3.2**) and hence other models are also checked. The square of the correlation coefficient (R^2) values, for different initial MB concentrations, are much lower than one and hence denies the appropriateness of the pseudo-first order kinetic model. This is also confirmed due to distinct variations in the value of experimentally obtained Q_e and theoretically obtained Q_e (**Table 3.2**).

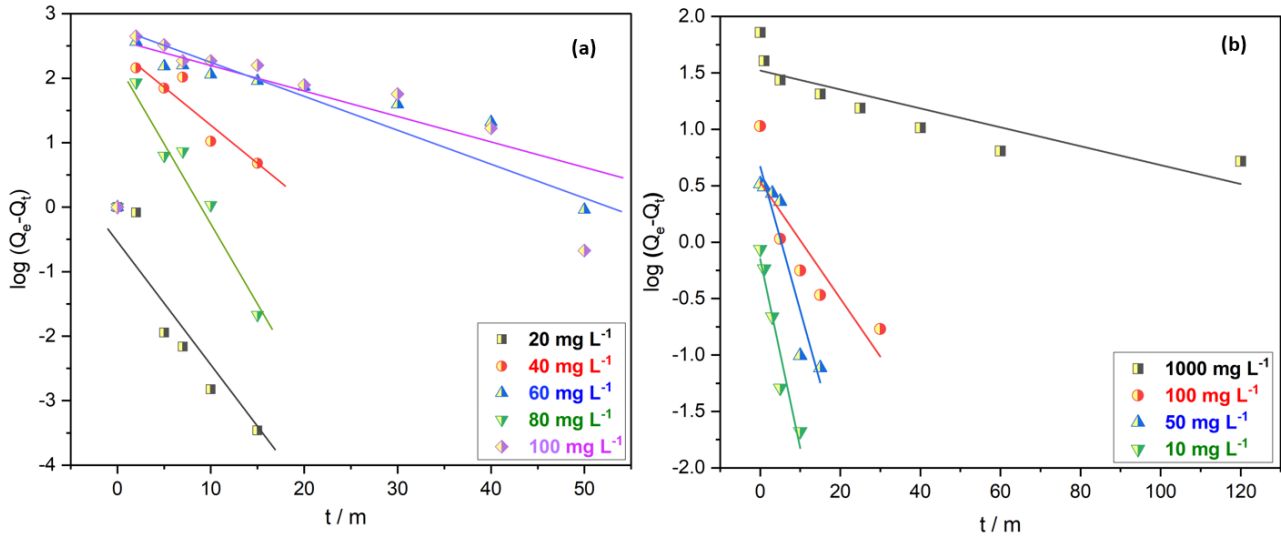


Figure 3.11: Variation of $\log(Q_e - Q_i)$ vs t and fitted data of Pseudo-first order kinetic model: a) DES-GO@ZrO₂ (2 mg/ml dosage, 20 ml solution of MB), and b) CGS-GO@ZrO₂ (10 mg/ml dosage, 20 ml solution of MB) at $30 \pm 0.1^\circ\text{C}$.

Table 3.2: Fitted kinetic data in different models for DES-GO@ZrO₂ and CGS-GO@ZrO₂

DES-GO@ZrO ₂										
Adsorbent (mg/L)	Pseudo-first order				Pseudo-second order			Intra-particle diffusion		
	$Q_e(\text{exp})$ (mg g ⁻¹)	$Q_e(\text{cal})$ (mg g ⁻¹)	K_1 (min ⁻¹)	R^2	$Q_e(\text{cal})$ (mg g ⁻¹)	K_2 (g mg ⁻¹ min ⁻¹)	R^2	K_i	C_i	R^2
20	9.88	9.92	0.087	0.885	9.94	1.065	0.999	2.412	2.69	0.620
40	19.93	18.76	0.035	0.239	20.99	0.019	0.993	2.272	5.88	0.765
60	29.84	22.55	0.596	0.113	31.66	0.033	0.967	2.197	5.99	0.921
80	39.89	23.56	0.113	0.387	41.52	0.004	0.979	2.687	11.21	0.857
100	47.85	25.36	0.067	0.209	54.43	0.001	0.896	3.584	3.02	0.968
CGS-GO@ZrO ₂										
Adsorbent (mg/L)	Pseudo-first order				Pseudo-second order			Intra-particle diffusion		
	$Q_e(\text{exp})$ (mg g ⁻¹)	$Q_e(\text{cal})$ (mg g ⁻¹)	K_1 (min ⁻¹)	R^2	$Q_e(\text{cal})$ (mg g ⁻¹)	K_2 (g mg ⁻¹ min ⁻¹)	R^2	K_i	C_i	R^2
10	0.86	0.745	0.011	0.909	0.98	0.668	0.988	0.233	0.10	0.603
50	3.28	3.184	0.063	0.864	33.70	0.001	0.913	0.897	0.47	0.529
100	9.33	10.14	0.011	0.655	10.81	0.154	0.999	1.395	3.55	0.861
1000	72.13	58.35	0.034	0.716	72.83	0.002	0.998	3.663	28.71	0.825

3.3.9.2 Pseudo-second order kinetic model

In the process of finding the correctness of the kinetic model the data of MB adsorption, with both NCs, were fitted in pseudo-second order kinetic equation [73],

$$\frac{t}{Q_t} = \frac{1}{k_2 Q_e^2} + \frac{t}{Q_e} \quad (2)$$

where k_2 ($\text{g mg}^{-1} \text{min}^{-1}$), the second order rate constant, and Q_e have been computed from a straight-line plot (**Figure 3.12 (a & b)**) of t/Q_t vs t (using slope and intercept). When $t \rightarrow 0$, the adsorption rate becomes the initial adsorption speed. The data computed for this model are compiled in **Table 3.2**. Better R^2 values (~ 1) indicate the suitability of the pseudo-second order kinetic model to understand the adsorption kinetics of MB on both modified NCs (CGS-GO@ZrO₂ and DES-GO@ZrO₂).

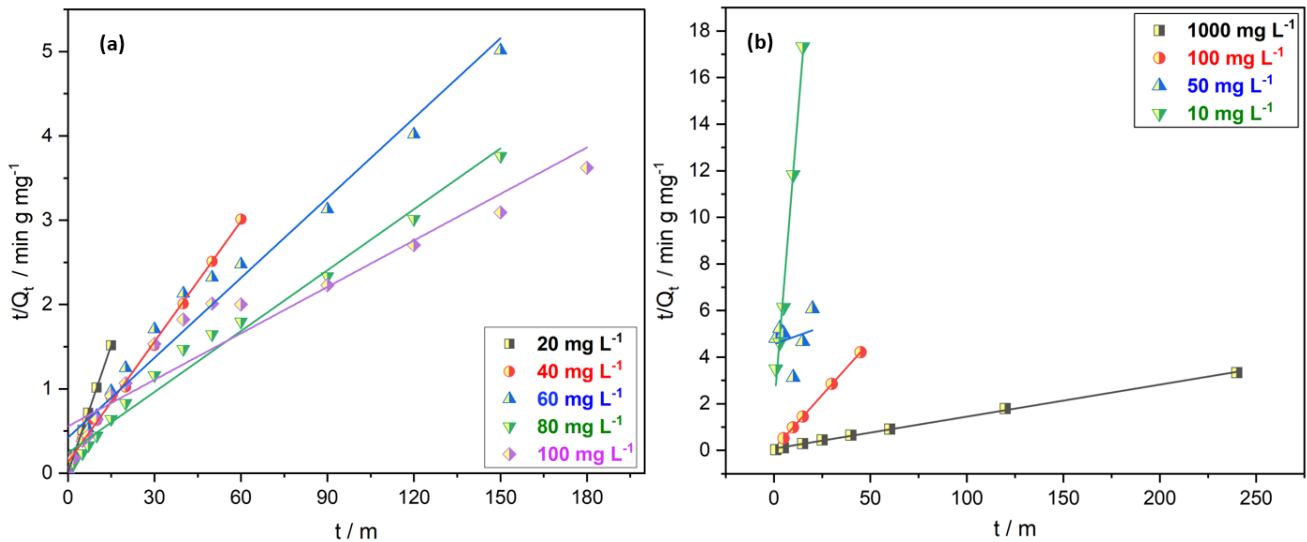


Figure 3.12: Variation of t/Q_t vs t and fitted data of Pseudo-second order kinetic model: a) DES-GO@ZrO₂ (2 mg/ml dosage, 20 ml solution of MB), and b) CGS-GO@ZrO₂ (10 mg/ml dosage, 20 ml solution of MB) at $30 \pm 0.1^\circ\text{C}$.

3.3.9.3 Intraparticle diffusion kinetic model

Another kinetic model has also been used to interpret adsorption behaviour. This model also considers the diffusion process of adsorbate in addition to concentration variation. The well-known expression [74] of the present model is as follows,

$$Q_t = k_i t^{1/2} + C_i \quad (3)$$

k_i is the intraparticle velocity constant ($\text{mg g}^{-1} \text{min}^{1/2}$) and C_i is a constant that is related to boundary layer thickness/diffusion. If Q_t vs $t^{1/2}$ provides a linear plot (**Figure 3.13 (a & b)**) whose slope and intercept can be used to obtain k_i and C_i . The computed values of k_i , C_i , and R^2 are summarized in **Table 3.2**. Looking at the fitted data and R^2 values (far less than 1), one can be observed that pore/surface diffusion is not the only factor but other routes such as film diffusion may also involve.

From a perusal of all the fitted data in different kinetic models with both the NCs (Table 3.2), it can be seen that better fitting (Figure 3.13) and acceptable R² values are produced with Pseudo-second order kinetic model and hint that this model is probably followed in the present adsorption of MB on both the modified NCs surfaces.

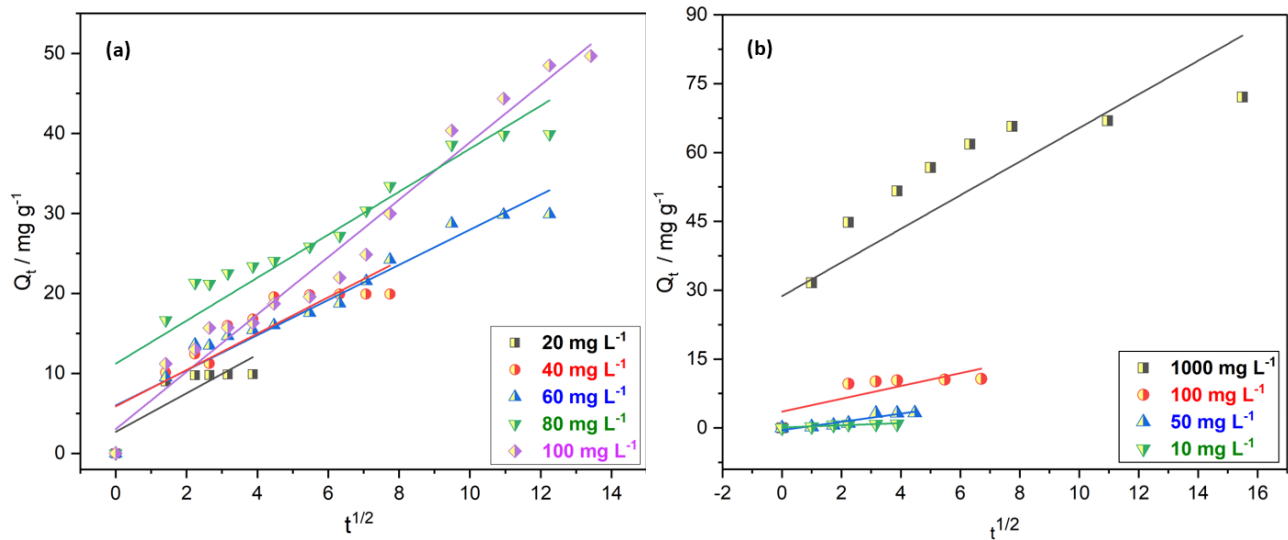


Figure 3.13: Variation of Q_t vs $t^{1/2}$ and fitted data of Intraparticle diffusion kinetic model: a) DES-GO@ZrO₂ (2 mg/ml dosage, 20 ml solution of MB), and b) CGS-GO@ZrO₂ (10 mg/ml dosage, 20 ml solution of MB) at 30±0.1°C.

3.3.10 Adsorption isotherm

The applicability of different adsorption isotherm models (at 30±0.1°C) has been checked by considering Freundlich, Langmuir, and Temkin.

3.3.10.1 Freundlich isotherm

According to this adsorption model, the surface of the composite is heterogeneous and assists in multilayer adsorption. Mathematically, Freundlich isotherm model can be expressed [75] as under,

$$\log Q_e = \log K_{FI} + \frac{1}{n} \log C_e \quad (5)$$

where K_{FI} (mg/g) and n are the Freundlich adsorption constant and adsorption potency, respectively. n decides the spontaneity and reversibility of the process ($0 < 1/n < 1$, spontaneous; $1/n > 1$, non-spontaneous; $1/n = 1$, non-reversible). K_{FI} and n can be computed from the intercept and slope of the plots of $\log Q_e$ vs $\log C_e$ (Figure 3.14) where C_e is the equilibrium [MB]. The related data are summarized in Table 3.3. The poor R² values clearly indicate the non-applicability of Freundlich adsorption model and deny the multilayer adsorption.

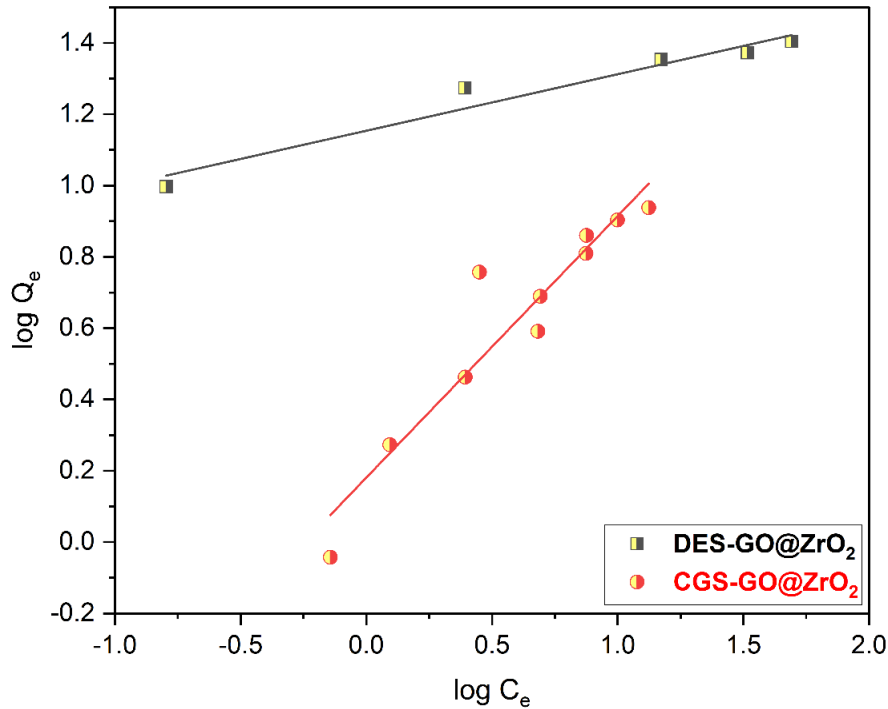


Figure 3.14: Variation of $\log Q_e$ vs $\log C_e$ and fitted Freundlich isotherm model for DES-GO@ZrO₂ (2 mg/ml dosage, 20 ml solution of MB), and CGS-GO@ZrO₂ (10 mg/ml dosage, 20 ml solution of MB) at $30 \pm 0.1^\circ\text{C}$.

Table 3.3: Fitted adsorption data of MB on DES-GO@ZrO₂ and CGS-GO@ZrO₂ using various models.

Isotherms	Parameters	DES-GO@ZrO ₂	CGS-GO@ZrO ₂
<i>Freundlich</i>	K_{FI} (mg/g)	14.24	1.51
	n	0.15	0.73
	R^2	0.936	0.885
<i>Langmuir</i>	Q_m (mg/g)	22.94	15.91
	b (L/mg)	4.731	0.127
	R^2	0.971	0.995
	R_{EP}	0.0104-0.0021	0.4405-0.0078
<i>Temkin</i>	K_T (L/g)	359.50	3.50
	2.303 RT/b	2.595	2.251
	R^2	0.979	0.816

3.3.10.2 Langmuir isotherm

Since Freundlich adsorption isotherm model fails to fit the present adsorption data of MB and, therefore, other models were tried to know the exact mechanism of MB adsorption. Another well-known adsorption model namely, Langmuir isotherm [76], has been considered to fit. The Langmuir isotherm is represented by,

$$\frac{1}{Q_e} = \frac{1}{Q_m} \times \frac{1}{b} \times \frac{1}{C_e} + \frac{1}{Q_m} \quad (8)$$

where Q_m is the content of MB to form uni-layer (mg/g) and b (L/mg) constant which represents adsorption energy. A plot of $1/Q_e$ vs $1/C_e$ results straight line with slope (gives $1/b \cdot Q_m$) and intercept ($1/Q_m$) (**Figure 3.15**). The values of R^2 were found reasonably good and compiled with other adsorption constants of this model in **Table 3.3**. These data indicate the suitability of Langmuir model for the MB adsorption on modified NCs. This was further confirmed by the determination of the equilibrium adsorption parameter (R_{EP}) which is related to b and C_i by the following mathematical expression,

$$R_{EP} = \frac{1}{1+bC_i} \quad (9)$$

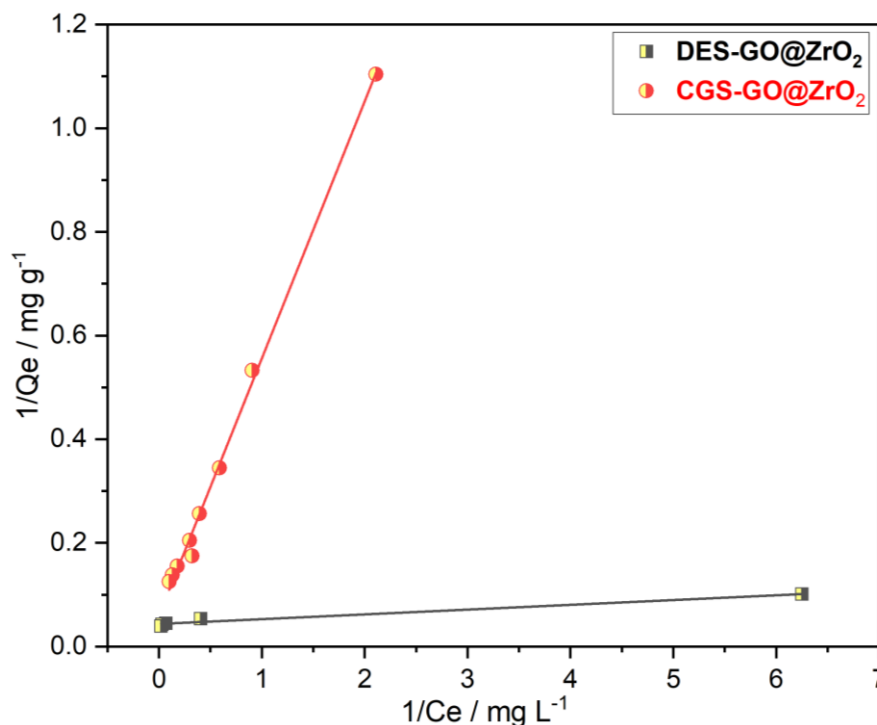


Figure 3.15: Variation of $1/Q_e$ vs $1/C_e$ and fitted Langmuir isotherm model for DES-GO@ZrO₂ (2 mg/ml dosage, 20 ml solution of MB), and CGS-GO@ZrO₂ (10 mg/ml dosage, 20 ml solution of MB) at $30 \pm 0.1^\circ\text{C}$.

R_{EP} gives an idea about the favorability of adsorption equilibrium. The ranges of R_{EP} for different initial [MB] are also tabulated in **Table 3.3**. R_{EP} varies between 0.01 to 0.0021 (for DES-GO@ZrO₂) and 0.4405-0.0078 (for CGS-GO@ZrO₂) which proves that monolayer adsorption is taking place spontaneously. Further, NCs provide nearly homogeneous surfaces.

3.3.10.3 Temkin isotherm

To ensure the applicability of Langmuir model, the adsorption data were also fitted into another well-known model, known as Temkin isotherm [77]. This model asserts that the heat of adsorption lowers linearly during the transfer of adsorbate toward the adsorbent surface. the model can be expressed mathematically as,

$$Q_e = 2.303 \frac{RT}{b} (\log K_T + \log C_e) \quad (10)$$

The term K_T (L/g) is the Temkin constant related to the energy involved in the binding of MB to modified NC. The value of RT/b gives insight into the nature of the adsorption process. These values were obtained from the slope and intercept of the plot of Q_e vs $\log C_e$ (**Figure 3.16**). If $RT/b > 0$, the process can be said exothermic and vice versa while $RT/b < 0$, which means that heat is absorbed during adsorption, i.e., an endothermic process. The values of RT/b , K_T , and R^2 are also included in **Table 3.3**.

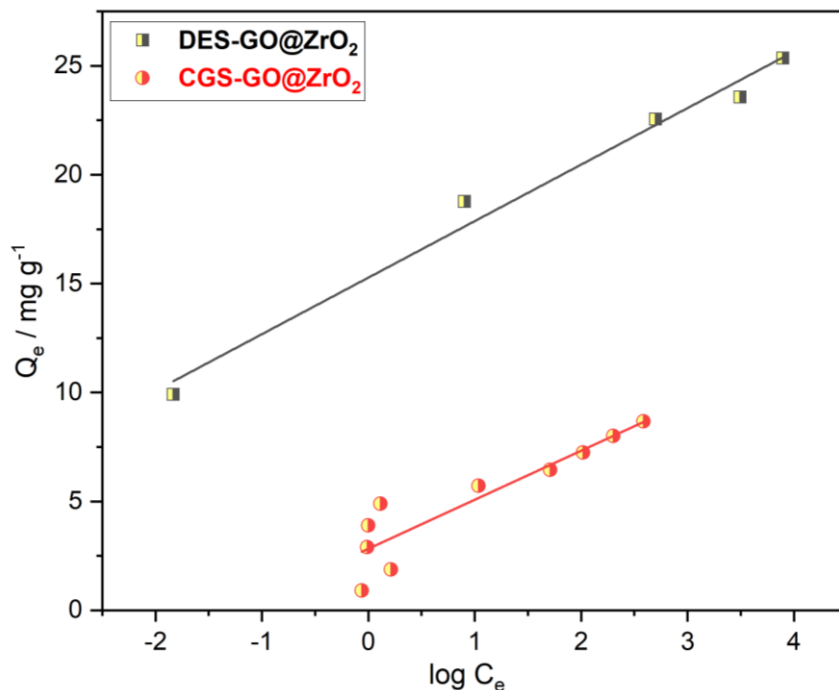


Figure 3.16: Variation of Q_e vs $\log C_e$ and fitted Temkin isotherm model for DES-GO@ZrO₂ (2 mg/ml dosage, 20 ml solution of MB), and CGS-GO@ZrO₂ (10 mg/ml dosage, 20 ml solution of MB) at $30 \pm 0.1^\circ\text{C}$.

A perusal of isotherm parameters (Table 3.3) of different adsorption models (mentioned above) indicates that both Langmuir (monolayer adsorption) and Temkin (exothermic) models are equally followed by the MB adsorption data obtained with CGS-GO@ZrO₂ and DES-GO@ZrO₂ as adsorbents. This indicates that monolayer adsorption of MB is taking place together with a heat release. Therefore, the binding strength of MB to DES-GO@ZrO₂ seems higher than CGS-GO@ZrO₂.

3.3.11 Comparison of MB adsorption with similar composite material

Table 3.4 shows the compilation of the adsorption/removal data of MB with similar composites [78–81]. Among two modified composites (for faster removal), DES-GO@ZrO₂ has been found superior to CGS-GO@ZrO₂. A perusal of comparative data shows that DES-GO@ZrO₂ shows good adsorption efficiency (close to 100 %) within a short time (5 m) through the DES-GO@ZrO₂ dose was slightly towards the higher side. However, the adsorption time column of Table 3.4 clearly depicts that the DES-GO@ZrO₂ can be a preferred candidate for the faster removal of MB or similar material (yet to be checked). Based on this observation, DES-GO@ZrO₂ has been chosen for the recyclability study.

Table 3.4: Comparison of removal efficiency of DES-GO@ZrO₂ and CGS-GO@ZrO₂ with similar materials reported in the literature.

Nanocomposite Names	Adsorbent Dosage (mg/mL)	Initial MB Concentration (ppm)	Adsorption Time (min)	Removal Efficiency (%)	References
DES-GO@ZrO ₂	2	20	5	~100 %	This work
CGS-GO@ZrO ₂	10	10	5	82 %	
Fe ₃ O ₄ -xGO	0.28	150	180	97.5 %	[78]
CS/Fe ₃ O ₄ /GO	0.4	5	1200	~25 %	[80]
MGC/GO	1	30	840	96.7 %	[79]
GO/Fe ₃ O ₄ /SiO ₂	0.25	3.2	10	~65 %	[81]

3.3.12 Recyclability/Reusability Study

For an adsorbent, the potential is not only counted by its adsorption/removal efficiency but also by reusability (to control the economy of the process) one after another cycle [82–84]. Here, MB adsorbed DES-GO@ZrO₂ has been recycled by washing it with various solvents (water, 0.1M HCl, 0.1M NaOH, methanol, and ethanol). The washing ability of adsorbed MB has been shown in Figure 3.18. Ethanol has been found better solvent to desorb MB from the said composite (R_e~86%). Figure 3.17 shows the adsorption-desorption efficacy of the MB adsorbed DES-GO@ZrO₂. It can be noticed that the composite can be efficiently recycled/reused for at

least 5 successive cycles with ethanol as the recharging solvent. The efficiency of the process corroborates the physical interaction involved in the adsorption process of MB. Better adsorption capabilities even after 5 cycles suggest that the DES-GO@ZrO₂ can perform as a potential adsorbent for MB or MB derivatives [85].

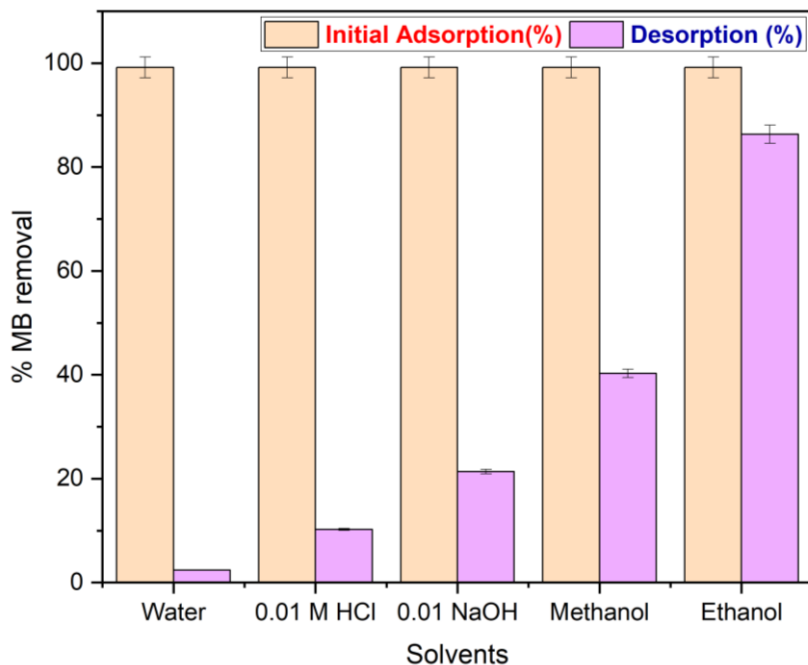


Figure 3.17: Desorption study of MB from DES-GO@ZrO₂ using 50 ml of various solvents.

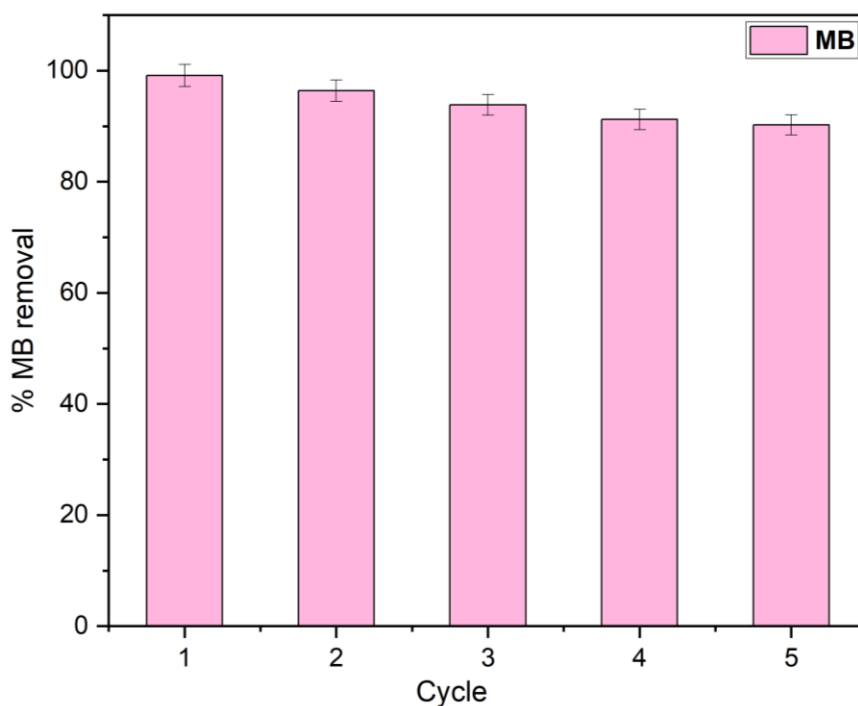
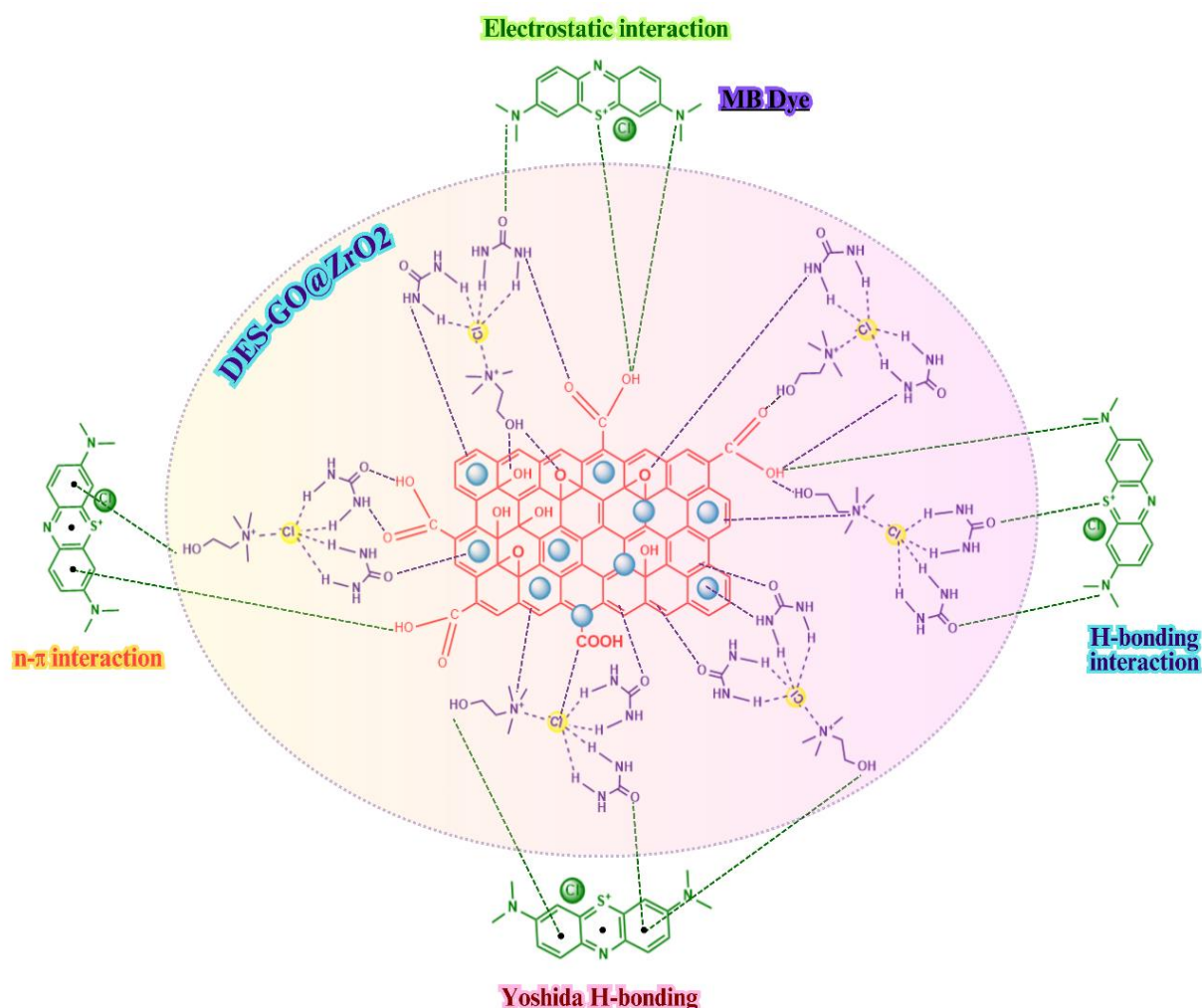
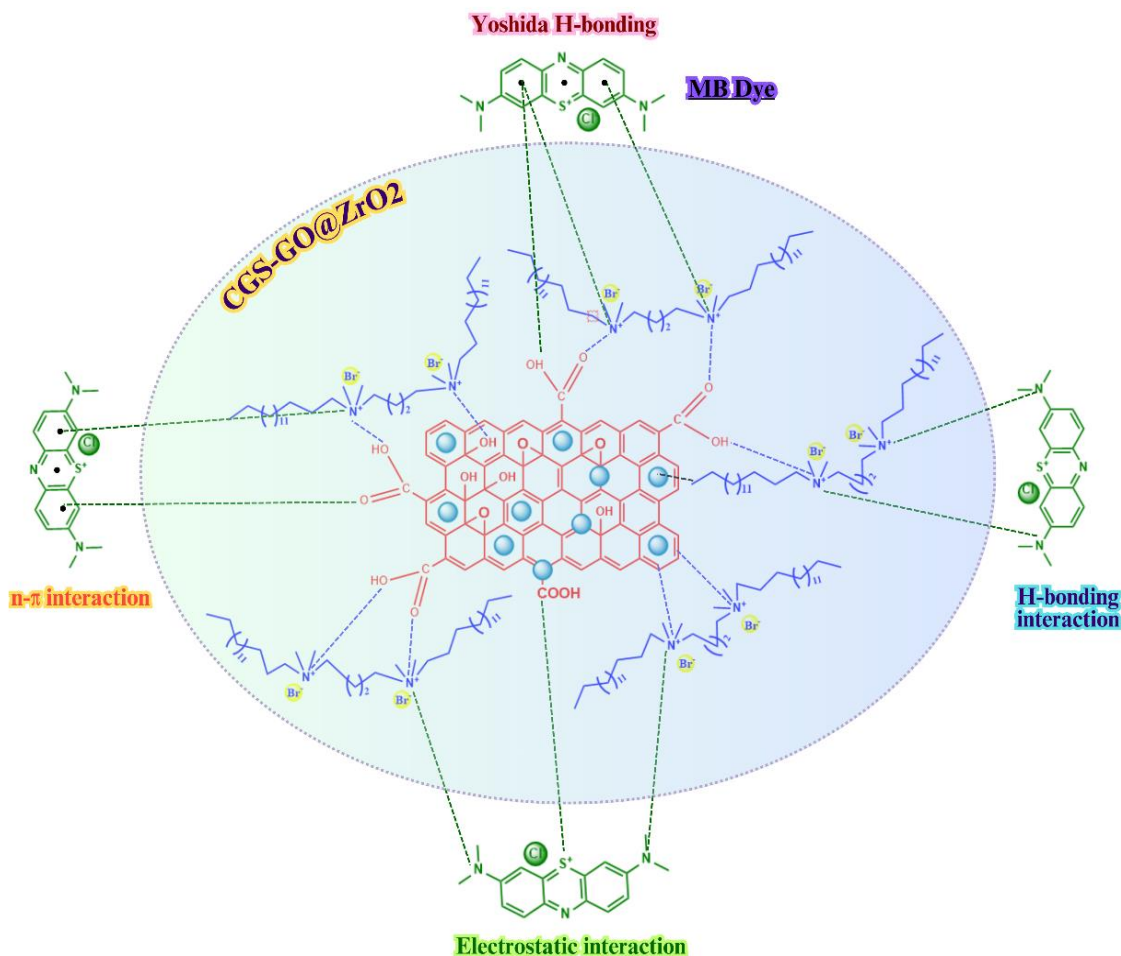


Figure 3.18: Recyclability study of DES-GO@ZrO₂ using 50 ml of ethanol for each cycle (up to 5 cycles).

3.3.13 Mechanism of MB adsorption

Preliminary TEM data (Figure 3.3) show that ZrO₂ sits on the surface of GO sheets with a homogenous distribution. CGS and DES contain certain groups which can interact with GO@ZrO₂ composite via electrostatic and hydrophobic interaction. MB will be adsorbed on the modified surface of the composite via various interactions represented in Scheme 3.1. Various active groups are available on the modified NCs which perform an important role in the MB adsorption process. The nature of the NCs is shifted towards hydrophobic (due to hydrocarbon chains available on CGS or DES) which consequently contributes to attracting MB molecules towards the adsorbent surface.





Scheme 3.1: Depiction of MB adsorption on modified NCs via different modes of interactions.

3.4 Conclusion

In conclusion, DES-GO@ZrO₂ has been found distinctly better than CGS-GO@ZrO₂ for the adsorption/removal from an aqueous solution of MB. The adsorption process has been found to be driven by electrostatic/hydrophobic interactions of MB with NC surfaces. Results of the adsorption process follow Langmuir adsorption isotherm indicating the homogeneity of the NC surfaces. DES-GO@ZrO₂ shows complete adsorption (within 5 m) for MB when compared with other similar adsorbents (**Table 3.4**). Kinetic study showed that adsorption-time data follow *pseudo*-second order kinetics. The recyclability experiment showed that DES-GO@ZrO₂ performs well even after the 5th cycle. Ethanol has been found good recharging solvent for the said composite. Further, the information can be used to produce potential commercial filters involving DES-GO@ZrO₂ for the faster/effective removal of coloured dyes or colouring material before discarding into running streams (control of water pollution to make it potable for humans, aquatic habitats together with irrigation). The spectrum of application can be enlarged by performing similar studies with other industrial effluents *e.g.*, paint, textile, leather, or paper.

3.5 References

- [1] R. K. Joshi, S. Alwarappan, M. Yoshimura, V. Sahajwalla, and Y. Nishina, *Appl Mater Today* **1**, 1 (2015).
- [2] S. Maniappan, C. Dutta, D. M. Solís, J. M. Taboada, and J. Kumar, *Angewandte Chemie International Edition* (2023).
- [3] N. Baig, I. Kammakakam, and W. Falath, *Mater Adv* **2**, 1821 (2021).
- [4] A. Ambrosi, C. K. Chua, N. M. Latiff, A. H. Loo, C. H. A. Wong, A. Y. S. Eng, A. Bonanni, and M. Pumera, *Chem Soc Rev* **45**, 2458 (2016).
- [5] M. Francisco, A. van den Bruinhorst, and M. C. Kroon, *Angewandte Chemie International Edition* **52**, 3074 (2013).
- [6] A. Paiva, R. Craveiro, I. Aroso, M. Martins, R. L. Reis, and A. R. C. Duarte, *ACS Sustain Chem Eng* **2**, 1063 (2014).
- [7] X. Li, Y.-L. Wang, J. Wen, L. Zheng, C. Qian, Z. Cheng, H. Zuo, M. Yu, J. Yuan, R. Li, W. Zhang, and Y. Liao, *Nat Commun* **14**, 263 (2023).
- [8] R. Zana and Y. Talmon, *Nature* **362**, 228 (1993).
- [9] R. von Ballmoos and W. M. Meier, *Nature* **289**, 782 (1981).
- [10] R. D. Rogers, *Nature* **447**, 917 (2007).
- [11] B. Boates, A. M. Teweldeberhan, and S. A. Bonev, *Proceedings of the National Academy of Sciences* **109**, 14808 (2012).
- [12] B. F. Machado and P. Serp, *Catal. Sci. Technol.* **2**, 54 (2012).
- [13] X. Huang, X. Qi, F. Boey, and H. Zhang, *Chem. Soc. Rev.* **41**, 666 (2012).
- [14] L. Jiao, L. Zhang, X. Wang, G. Diankov, and H. Dai, *Nature* **458**, 877 (2009).
- [15] O. V. Yazyev and S. G. Louie, *Nat Mater* **9**, 806 (2010).
- [16] C. Cheng and D. Li, *Advanced Materials* **25**, 13 (2013).
- [17] I. Chowdhury, M. C. Duch, N. D. Mansukhani, M. C. Hersam, and D. Bouchard, *Environ Sci Technol* **47**, 6288 (2013).
- [18] F. Mouhat, F.-X. Coudert, and M.-L. Bocquet, *Nat Commun* **11**, 1566 (2020).

- [19] Q. Zhou, J. Huang, J. Wang, Z. Yang, S. Liu, Z. Wang, and S. Yang, *RSC Adv* **5**, 91802 (2015).
- [20] N. Nasseh, F. S. Arghavan, N. Daglioglu, and A. Asadi, *Environmental Science and Pollution Research* **28**, 19222 (2021).
- [21] N. El-Shafai, M. E. El-Khouly, M. El-Kemary, M. Ramadan, I. Eldesoukey, and M. Masoud, *RSC Adv* **9**, 3704 (2019).
- [22] K. Thangavelu, C. Aubry, and L. Zou, *Ind Eng Chem Res* **60**, 1266 (2021).
- [23] K. Sanjeev Kumar, K. Giribabu, R. Suresh, R. Manigandan, S. Praveen Kumar, and V. Narayanan, *Mater Lett* **283**, 128804 (2021).
- [24] X. Kang, X. Zhu, J. Liu, X. Shu, Y. Huang, and J. Qian, *Compos B Eng* **186**, 107800 (2020).
- [25] N. Devi, R. Kumar, S. Singh, and R. K. Singh, *Critical Reviews in Solid State and Materials Sciences* **1** (2022).
- [26] R. S. Das, S. K. Warkhade, A. Kumar, G. S. Gaikwad, and A. V. Wankhade, *J Alloys Compd* **846**, 155770 (2020).
- [27] G. Z. Kyzas, E. A. Deliyanni, D. N. Bikiaris, and A. C. Mitropoulos, *Chemical Engineering Research and Design* **129**, 75 (2018).
- [28] H. W. Ha, A. Choudhury, T. Kamal, D.-H. Kim, and S.-Y. Park, *ACS Appl Mater Interfaces* **4**, 4623 (2012).
- [29] Y. Qi, M. Yang, W. Xu, S. He, and Y. Men, *J Colloid Interface Sci* **486**, 84 (2017).
- [30] Y. Kuang, R. Yang, Z. Zhang, J. Fang, M. Xing, and D. Wu, *Chemosphere* **236**, 124416 (2019).
- [31] W. M. Algothmi, N. M. Bandaru, Y. Yu, J. G. Shapter, and A. V. Ellis, *J Colloid Interface Sci* **397**, 32 (2013).
- [32] Z. Wu, H. Zhong, X. Yuan, H. Wang, L. Wang, X. Chen, G. Zeng, and Y. Wu, *Water Res* **67**, 330 (2014).
- [33] S. Singh, B. Patel, K. Parikh, and S. Kumar, *ChemistrySelect* **5**, 14230 (2020).
- [34] J. Yuan, A. Luna, W. Neri, C. Zakri, T. Schilling, A. Colin, and P. Poulin, *Nat Commun* **6**, 8700 (2015).

- [35] S. S. Basu, S. Rahut, A. S. Bisht, and J. K. Basu, *Mater Sci Semicond Process* **147**, 106681 (2022).
- [36] V. Agarwal, Y. Fadil, A. Wan, N. Maslekar, B. N. Tran, R. A. Mat Noor, S. Bhattacharyya, J. Biazik, S. Lim, and P. B. Zetterlund, *ACS Appl Mater Interfaces* **13**, 18338 (2021).
- [37] V. Georgakilas, M. Otyepka, A. B. Bourlinos, V. Chandra, N. Kim, K. C. Kemp, P. Hobza, R. Zboril, and K. S. Kim, *Chem Rev* **112**, 6156 (2012).
- [38] M. Yusuf, M. A. Khan, M. Otero, E. C. Abdullah, M. Hosomi, A. Terada, and S. Riya, *J Colloid Interface Sci* **493**, 51 (2017).
- [39] Y. Wu, H. Luo, H. Wang, C. Wang, J. Zhang, and Z. Zhang, *J Colloid Interface Sci* **394**, 183 (2013).
- [40] M. Yusuf, M. A. Khan, E. C. Abdullah, M. Elfgghi, M. Hosomi, A. Terada, S. Riya, and A. Ahmad, *Chemical Engineering Journal* **304**, 431 (2016).
- [41] K. Taleb, I. Pillin, Y. Grohens, and S. Saidi-Besbes, *Appl Clay Sci* **161**, 48 (2018).
- [42] S. Kalam, S. A. Abu-Khamsin, M. S. Kamal, S. M. S. Hussain, K. Norrman, M. Mahmoud, and S. Patil, *Energy & Fuels* **36**, 5737 (2022).
- [43] H. Wang, R. Li, Q. Wu, G. Fei, Y. Li, M. Zou, and L. Sun, *Appl Surf Sci* **565**, 150581 (2021).
- [44] S. He, X. Liu, P. Yan, A. Wang, J. Su, and X. Su, *RSC Adv* **9**, 4908 (2019).
- [45] Y.-Y. Lyu, S. H. Yi, J. K. Shon, S. Chang, L. S. Pu, S.-Y. Lee, J. E. Yie, K. Char, G. D. Stucky, and J. M. Kim, *J Am Chem Soc* **126**, 2310 (2004).
- [46] S. K. Yadav, K. Parikh, and S. Kumar, *Colloids Surf A Physicochem Eng Asp* **522**, 105 (2017).
- [47] S. Chen, W. Wang, and W. Xu, *Mater Lett* **180**, 196 (2016).
- [48] B. B. Hansen, S. Spittle, B. Chen, D. Poe, Y. Zhang, J. M. Klein, A. Horton, L. Adhikari, T. Zelovich, B. W. Doherty, B. Gurkan, E. J. Maginn, A. Ragauskas, M. Dadmun, T. A. Zawodzinski, G. A. Baker, M. E. Tuckerman, R. F. Savinell, and J. R. Sangoro, *Chem Rev* **121**, 1232 (2021).
- [49] M. Rabiul Islam, F. Warsi, M. Sayem Alam, and M. Ali, *J Mol Liq* **334**, 116483 (2021).
- [50] F. Warsi, M. R. Islam, M. S. Alam, and M. Ali, *J Mol Liq* **310**, 113132 (2020).

- [51] M. R. Islam, S. Shakya, A. Selim, M. S. Alam, and M. Ali, *J Chem Eng Data* **64**, 4169 (2019).
- [52] Y. Huang, Y. Wang, Q. Pan, Y. Wang, X. Ding, K. Xu, N. Li, and Q. Wen, *Anal Chim Acta* **877**, 90 (2015).
- [53] N. Mehrabi, H. Lin, and N. Aich, *Chemical Engineering Journal* **412**, 128577 (2021).
- [54] M. A. Shannon, P. W. Bohn, M. Elimelech, J. G. Georgiadis, B. J. Mariñas, and A. M. Mayes, *Nature* **452**, 301 (2008).
- [55] C. Tortajada and P. van Rensburg, *Nature* **577**, 26 (2020).
- [56] B. Van der Bruggen, *Nat Rev Chem* **5**, 217 (2021).
- [57] D. Hoornweg, P. Bhada-Tata, and C. Kennedy, *Nature* **502**, 615 (2013).
- [58] W. J. Cosgrove and D. P. Loucks, *Water Resour Res* **51**, 4823 (2015).
- [59] X.-Z. Tang, Z. Cao, H.-B. Zhang, J. Liu, and Z.-Z. Yu, *Chemical Communications* **47**, 3084 (2011).
- [60] A. Ahmad, S. N. A. Md. Jamil, T. S. Y. Choong, A. H. Abdullah, N. H. Faujan, A. A. Adeyi, R. Daik, and N. Othman, *Polymers (Basel)* **14**, 5416 (2022).
- [61] A. P. Nambiar, R. Pillai, Y. Vadikkeetil, M. Sanyal, and P. S. Shrivastav, *Mater Chem Phys* **291**, 126752 (2022).
- [62] A. H. Jawad, A. S. Abdulhameed, L. D. Wilson, M. A. K. M. Hanafiah, W. I. Nawawi, Z. A. ALOthman, and M. Rizwan Khan, *J Polym Environ* **29**, 2855 (2021).
- [63] J. Iqbal, N. S. Shah, M. Sayed, N. K. Niazi, M. Imran, J. A. Khan, Z. U. H. Khan, A. G. S. Hussien, K. Polychronopoulou, and F. Howari, *J Hazard Mater* **403**, 123854 (2021).
- [64] S. R. Lakhota, M. Mukhopadhyay, and P. Kumari, *Sci Rep* **8**, 4976 (2018).
- [65] E. L. Smith, A. P. Abbott, and K. S. Ryder, *Chem Rev* **114**, 11060 (2014).
- [66] J. Liu, X. Meng, Y. Hu, D. Geng, M. N. Banis, M. Cai, R. Li, and X. Sun, *Carbon N Y* **52**, 74 (2013).
- [67] X. Luo, C. Wang, L. Wang, F. Deng, S. Luo, X. Tu, and C. Au, *Chemical Engineering Journal* **220**, 98 (2013).
- [68] R. A. K. Rao, S. Singh, B. R. Singh, W. Khan, and A. H. Naqvi, *J Environ Chem Eng* **2**, 199 (2014).

- [69] T. Aissaoui, *Pharm Anal Acta* **6**, (2015).
- [70] J. T. Adeleke, T. Theivasanthi, M. Thirupathi, M. Swaminathan, T. Akomolafe, and A. B. Alabi, *Appl Surf Sci* **455**, 195 (2018).
- [71] N. Nasseh, F. S. Arghavan, N. Daglioglu, and A. Asadi, *Environmental Science and Pollution Research* **28**, 19222 (2021).
- [72] H. Yuh-Shan, *Scientometrics* **59**, 171 (2004).
- [73] A. E. Ofomaja, E. B. Naidoo, and S. J. Modise, *Desalination* **251**, 112 (2010).
- [74] V. Selen, Ö. Güler, D. Özer, and E. Evin, *Desalination Water Treat* **57**, 8826 (2016).
- [75] D. Robati, B. Mirza, M. Rajabi, O. Moradi, I. Tyagi, S. Agarwal, and V. K. Gupta, *Chemical Engineering Journal* **284**, 687 (2016).
- [76] Y. Liu, *Colloids Surf A Physicochem Eng Asp* **274**, 34 (2006).
- [77] M. Saxena, N. Sharma, and R. Saxena, *Surfaces and Interfaces* **21**, 100639 (2020).
- [78] L. Cui, X. Guo, Q. Wei, Y. Wang, L. Gao, L. Yan, T. Yan, and B. Du, *J Colloid Interface Sci* **439**, 112 (2015).
- [79] H. Shi, W. Li, L. Zhong, and C. Xu, *Ind Eng Chem Res* **53**, 1108 (2014).
- [80] H. V Tran, L. T. Bui, T. T. Dinh, D. H. Le, C. D. Huynh, and A. X. Trinh, *Mater Res Express* **4**, 035701 (2017).
- [81] S. Yang, T. Zeng, Y. Li, J. Liu, Q. Chen, J. Zhou, Y. Ye, and B. Tang, *J Nanomater* **2015**, 1 (2015).
- [82] C. Liu, A. M. Omer, and X. Ouyang, *Int J Biol Macromol* **106**, 823 (2018).
- [83] G. R. Mahdavinia, M. Soleymani, M. Sabzi, H. Azimi, and Z. Atlasi, *J Environ Chem Eng* **5**, 2617 (2017).
- [84] L. M. Sanchez, R. P. Ollier, and V. A. Alvarez, *Journal of Polymer Research* **26**, 142 (2019).
- [85] M. Wainwright, *Int J Antimicrob Agents* **16**, 381 (2000).